Crystal Structures, Modeling, and Dielectric Property Relationships of 2:1 Ordered $Ba_3MM'_2O_9$ (M = Mg, Ni, Zn; M′ = Nb, Ta) Perovskites

Michael W. Lufaso†

Ceramics Division, Materials Science and Engineering Laboratory, National Institute of Standards and Technology, Gaithersburg, Maryland 20899-8520

Received January 31, 2004. Revised Manuscript Received March 10, 2004

The preparation, modeled and refined crystal structures, and structure−dielectric property relationships of five $Ba_3MM'_2O_9$ (M = Mg, Ni, Zn; M′ = Nb, Ta) perovskites are reported. Crystal structure modeling was used to generate initial structure models for Rietveld refinements of the neutron powder diffraction data. Bond valence sums calculated from the bond distances indicate Ba−O bonds are compressed and the M−O and M′−O_6 bonds are expanded from ideal lengths. A shift of Ta^{5+} and Nb^{5+} out of center of the [M′O_6] octahedra forms three short and three long M′−O bonds. The octahedral distortion is driven by the asymmetry in the O bonding network and aided by the second-order Jahn−Teller distortion of the d^0 Nb^{5+} and Ta^{5+} cations. Differences in the atomic coordination environments in the crystal structures were utilized to propose crystal structure−dielectric property relationships. The coordination of the divalent B-site cation (M^{2+}) was correlated with the temperature coefficient of the resonant frequency (τ_f); a more under-bonded M^{2+} exhibited a more negative τ_f. Also, if the bond valences sums of the B-site cations were closer to the formal oxidations states, then a higher $Q\times f$ was observed.

Introduction

Dielectric ceramic materials are of considerable interest owing to their technically important properties and the relatively uncharted science surrounding the interactions between the crystal structures, chemistry, and useful physical properties. The dielectric ceramics are found as discrete components (e.g., dielectric resonators and filters) that are vital enabling devices in microwave communications systems.[1] There are few known ceramic materials that meet the rigorous dielectric property requirements for use in device applications.[2] The dielectric constant (ϵ) is only one of the key properties needing optimization; the temperature coefficient of the resonant frequency (τ_f) and dielectric loss (tan δ), often reported as the quality factor $Q = (\tan \delta)^{-1}$ or $Q\times f$ where f is the measurement frequency, are also critical properties. Obtaining optimal values of these three properties simultaneously is difficult; for example, high ϵ materials often possess a large τ_f and low Q.

Perovskites have been extensively investigated for use as microwave dielectric materials because of the outstanding and tuneable dielectric properties present in a number of compositions. In the perovskite structure (AMO_3) the A-site cation is located in the cavity formed by the corner-sharing network of [MO_6] octahedra. The fit of the A-site cation is described by the tolerance factor (tol.).[3] If the tolerance factor is greater than unity, often no octahedral tilting is observed, whereas compositions with a tolerance factor less than unity typically undergo octahedral tilting distortions.[4,5] The series of $Ba_3MM'_2O_9$ (M = Mg, Ni, Zn; M′ = Nb, Ta) perovskites that do not undergo an octahedral tilting distortion exhibit optimal dielectric properties. The perovskites $Ba_3MgTa_2O_9$ (BMT) and $Ba_3ZnTa_2O_9$ (BZT) possess high $Q\times f$ values and a near zero τ_f.[6,7] The type of cation order influences the dielectric properties, with 2:1 order of the M and M′ cations exhibiting a larger $Q\times f$ than 1:1 ordered and disordered perovskites.[7−9] Substitutions on the A-, M-, and M′-site have been made extensively, but no alternative compounds have emerged for high-Q applications.[10−12] For example, B-site substitution of the identical ionic radius[13] (0.78 Å) Nb^{5+} for Ta^{5+} results in crystallization of isostructural 2:1 ordered perovskites; however, the ϵ is higher, Q is lower, and τ_f is more positive. The origins of the dielectric property differences between the isostructural compounds are not well-understood.

Entanglement of synthetic variables (e.g., chemical composition, reagent purity, annealing and sintering temperatures and times, initial particle size, processing

† E-mail: michael.lufaso@nist.gov.

(1) Vanderah, T. A. *Science* **2002**, *298*, 1182.
(2) Cava, R. J. *J. Mater. Chem.* **2001**, *11*, 54.
(3) Goldschmidt, V. M. *Naturwissenschaften* **1926**, *14*, 477.
(4) Glazer, A. M. *Acta Crystallogr., Sect. B* **1972**, *28*, 3384.
(5) Woodward, P. M. *Acta Crystallogr., Sect. B* **1997**, *53*, 32.
(6) Nomura, S.; Toyama, K.; Kaneta, K. *Jpn. J. Appl. Phys. 2* **1982**, *21*, L624.
(7) Kawashima, S.; Nishida, M.; Ueda, I.; Ouchi, H. *J. Am. Ceram. Soc.* **1983**, *66*, 421.
(8) Tamura, H.; Konoike, T.; Sakabe, Y.; Wakino, K. *J. Am. Ceram. Soc.* **1984**, *67*, C59.
(9) Akbas, M. A.; Davies, P. K. *J. Am. Ceram. Soc.* **1998**, *81*, 670.
(10) Hughes, H.; Iddles, D. M.; Reaney, I. M. *Appl. Phys. Lett.* **2001**, *79*, 2952.
(11) Thirumal, M.; Ganguli, A. K. *Bull. Mater. Sci.* **2002**, *25*, 259.
(12) Thirumal, M.; Ganguli, A. K. *Prog. Cryst. Growth Charact. Mater.* **2002**, 147.
(13) Shannon, R. D. *Acta Crystallogr., Sect. A* **1976**, *32*, 751.

10.1021/cm049831k
Published on Web 04/30/2004

conditions, and partial O_2 pressure) and experimental observables (e.g., crystal structure, density, cation order inside of a domain, ordered domain size, domain boundaries, defects, and impurity phases) that influence the dielectric properties (i.e., ϵ, τ_f, and Q) complicate formation of structure−property relationships. One structure−property relationship that has been developed strongly relates the incidence of octahedral tilting to the magnitude and sign of τ_f.[14−16] Substituting smaller A-site cations (i.e., A = Sr^{2+}, Ca^{2+}) in place of Ba^{2+} in $Ba_3MM'_2O_9$ perovskites is one approach to adjust the octahedral tilting and consequently the τ_f. Also, in general, a more negative temperature coefficient of the dielectric constant (τ_ϵ) (thus typically a more positive τ_f) is observed with an increase in ϵ.[17] The ϵ of dielectrics originates from the superposition of ionic and electronic polarization.[18] Electronic polarization is considered a constant for a particular ion, whereas ionic polarization occurs because of lattice vibrations related to the crystal structure and is a particularly important contribution in high ϵ (>20) materials.[19,20] Relationships between the crystal structure, dielectric properties, and crystal chemistry are prone to be complex; however, the elucidation of the structural differences between M′ = Ta and M′ = Nb compounds is a starting point in understanding the dielectric property differences.

Crystal structures reported in the literature indicate significant differences in the reported O fractional coordinates and cation coordination environments of BZT and BMT. The crystal structure of BZT was refined in space group $P\bar{3}m1$ from neutron powder diffraction data and recently refined with combined neutron and X-ray powder diffraction data.[21,22] The two crystal structures of BZT have significantly different B-site bond lengths (Å) [Zn−O 1.977(4) ×6, Ta−O 2.023(7) ×3, and 2.141(10) ×3][21] compared to [Zn−O 2.1246(22) ×6, Ta−O 1.9355(23) ×3, and 2.0827(13) ×3].[22,23] Similarly, the crystal structures of BMT refined from X-ray diffraction data show appreciably different B-site bond lengths (Å) [Mg−O 2.07(2) ×6, Ta−O 2.04(2) ×3, and 2.033(6) ×3][24,25] compared to [Mg−O 2.076(8) ×6, Ta−O 1.967(8) ×3, and 2.089(1) ×3].[26] Differences in the crystal structures of BMT may be partially attributed to the difficulty in refining accurate O positions from X-ray diffraction data. It is unclear from the reported crystal structures if Ta^{5+} shifts out of the center of the octahedra to form three short Ta−O bonds or retains long Ta−O bonds.

A group of five $Ba_3MM'_2O_9$ (M = Mg, Ni, Zn; M′ = Nb, Ta) perovskite compositions were synthesized and the crystal structures refined by the Rietveld method from neutron powder diffraction data. Idealized crystal structures were calculated by structure modeling in an effort to understand the differences in the reported crystal structures and to provide a starting structural model in the course of performing the Rietveld refinements. The $Ba_3MM'_2O_9$ compositions in this paper all have tolerance factors greater than unity and do not exhibit the added variable of octahedral tilting; therefore, these compositions are good candidates for extracting basic crystal structure−dielectric property relationships. A robust literature of dielectric characterization on these compositions was utilized to extend the suggested crystal structure−dielectric property relationships.

Experimental Methods

Sample Synthesis. Single-phase $Ba_3MgNb_2O_9$ (BMN), $Ba_3MgTa_2O_9$ (BMT), $Ba_3NiNb_2O_9$ (BNN), $Ba_3NiTa_2O_9$ (BNT), and $Ba_3ZnNb_2O_9$ (BZN) perovskite compounds were prepared by a MM'_2O_6 precursor route. Appropriate stoichiometric amounts of assayed $MgCO_3$ (Atomix), ZnO (Alfa Aesar, 99.99%), NiO (Alfa Aesar, 99.998%), Nb_2O_5 (Alfa Aesar, 99.9985%), and Ta_2O_5 (Alfa Aesar, 99.993%) were ground and then heated overnight at 1100 °C.[27] After the initial precursor heat cycle, a stoichiometric amount of $BaCO_3$ (Alfa Aesar, 99.95%) was added, intimately mixed, and calcined overnight to decompose the carbonate. Prior to each heat cycle, the samples were ground with an agate mortar and pestle, pelletized using a uniaxial press, and placed on sacrificial powder of the same composition on Pt foil on an alumina plate. The samples were covered with an inverted zirconia crucible prior to each heat cycle. These synthetic precautions were employed to suppress cation volatility and avoid formation of competing phases. In the synthesis of BZN the pellet was covered with a powder of the same composition and surrounded with a small excess of ZnO, which increases the ZnO partial pressure, to minimize Zn loss. Multiple (eight to nine) heat cycles, with intermediate grinding and repelletizing, were performed at increasing temperatures from 1100 °C to a final temperature of 1525 °C (BMN), 1575 °C (BMT), 1375 °C (BNN), 1475 °C (BNT), and 1250 °C (BZN).

Diffraction Data Collection. Phase purity was ascertained using X-ray powder diffraction data collected Cu Kα X-ray radiation with a Philips diffractometer equipped with incident Soller slits, theta compensating divergence slit, graphite monochromator, and scintillation detector. Equilibrium was assumed to occur when no further changes were evident in the relative intensities of the weak superlattice peaks associated with cation ordering and *c*/*a* lattice parameter ratio. Neutron powder diffraction data were collected using the BT-1 32 detector neutron powder diffractometer at the NCNR, NBSR. The samples were loaded in vanadium can sample containers of length 50 mm and diameter 12.4 mm. A Cu(311) monochromator with a 90° takeoff angle, $\lambda = 1.5402(2)$ Å, and in-pile collimation of 15 min of arc were used. Data were collected under ambient conditions over the range of 3°−168° 2θ with a step size of 0.05°. The instrument is described in the NCNR Web site (http://www.ncnr.nist.gov/).

Crystal Structure Modeling. The SPuDS modeling software,[28] which has been used to calculate the crystal structures

(14) Colla, E. L.; Reaney, I. M.; Setter, N. *J. Appl. Phys.* **1993**, *74*, 3414.
(15) Colla, E. L.; Reaney, I. M.; Setter, N. *Ferroelectrics* **1992**, *133*, 217.
(16) Reaney, I. M.; Colla, E. L.; Setter, N. *Jpn. J. Appl. Phys. 1* **1994**, *33*, 3984.
(17) Harrop, P. J. *J. Mater. Sci.* **1969**, *4*, 370.
(18) Shannon, R. D. *J. Appl. Phys.* **1993**, *73*, 348.
(19) Tamura, H.; Sagala, D. A.; Wakino, K. *Jpn. J. Appl. Phys. 1* **1986**, *25*, 787.
(20) Reaney, I. M.; Qazi, I.; Lee, W. E. *J. Appl. Phys.* **2000**, *88*, 6708.
(21) Jacobson, A. J.; Collins, B. M.; Fender, B. E. F. *Acta Crystallogr., Sect. B* **1976**, *32*, 1083.
(22) Bieringer, M.; Moussa, S. M.; Noailles, L. D.; Burrows, A.; Kiely, C. J.; Rosseinsky, M. J.; Ibberson, R. M. *Chem. Mater.* **2003**, *15*, 586.
(23) Crystal structure of the BZT-f powder sample.
(24) Vincent, H.; Perrier, C.; Lheritier, P.; Labeyrie, M. *Mater. Res. Bull.* **1993**, *28*, 951.
(25) Crystal structure of the nonsintered (polycrystalline) sample.
(26) Janaswamy, S.; Murthy, G. S.; Dias, E. D.; Murthy, V. R. K. *Mater. Lett.* **2002**, *55*, 414.

(27) Certain commercial equipment, instruments, or materials are identified in this paper to specify the experimental procedure adequately. Such identification is not intended to imply recommendation or endorsement by the National Institute of Standards and Technology, nor is it intended to imply that the materials or equipment identified are necessarily the best available for the purpose.

(28) Lufaso, M. W.; Woodward, P. M. *Acta Crystallogr., Sect. B* **2001**, *57*, 725.

Table 1. Predicted Structural Parameters and Bond Valence Sums (v.u.) and M^{5+}−O Bond Distances (Å) Obtained from SPuDS Calculations[a]

	$Ba_3MgNb_2O_9$	$Ba_3MgTa_2O_9$	$Ba_3NiNb_2O_9$	$Ba_3NiTa_2O_9$	$Ba_3ZnNb_2O_9$	$Ba_3ZnTa_2O_9$
tol.	1.033	1.030	1.039	1.036	1.031	1.028
a (Å)	5.830(1)	5.836(1)	5.820(1)	5.825(1)	5.835(1)	5.838(1)
c (Å)	7.142(1)	7.147(1)	7.131(1)	7.135(1)	7.142(1)	7.153(1)
c/*a*	1.2250	1.2247	1.2252	1.2250	1.2241	1.2251
Ba *z*	0.6799(1)	0.6793(1)	0.6813(1)	0.6807(1)	0.6795(1)	0.6788(1)
M^{5+} *z*	0.1800(1)	0.1805(1)	0.1833(1)	0.1838(1)	0.1791(1)	0.1794(1)
O2 *x*	0.1768(1)	0.1759(1)	0.1760(1)	0.1751(1)	0.1771(1)	0.1762(1)
O2 *z*	0.3251(1)	0.3258(1)	0.3265(1)	0.3273(1)	0.3246(1)	0.3254(1)
Ba1 (v.u.)	2.15	2.13	2.17	2.16	2.14	2.13
Ba2 (v.u.)	2.21	2.19	2.25	2.23	2.20	2.18
M^{2+} (v.u.)	1.61	1.65	1.52	1.56	1.64	1.68
M^{5+} (v.u.)	4.89	4.90	4.88	4.88	4.90	4.91
O1 (v.u.)	1.96	1.96	1.94	1.95	1.96	1.97
O2 (v.u.)	2.02	2.01	2.02	2.02	2.02	2.01
M^{5+}−O1 (×3) (Å)	2.117(1)	2.122(1)	2.129(1)	2.132(1)	2.115(1)	2.119(1)
M^{5+}−O2 (×3) (Å)	1.890(1)	1.900(1)	1.886(1)	1.897(1)	1.891(1)	1.902(1)

[a] The fixed atomic positions are given in the text.

of single B-site and 1:1 ordered B-site cation perovskites, has been modified to calculate the crystal structures of untilted 2:1 ordered B-site cation perovskites. Details of the calculation algorithm have been previously described; however, changes were made to the algorithm that allows the octahedra to undergo a distortion of bond lengths and angles. Instead of optimizing the anion position based on equations of octahedral tilting, the first coordination environment of each atom on an independent Wyckoff site was optimized within the symmetry constraints of space group $P\bar{3}m1$. The Wyckoff site (brackets) and atomic fractional coordinate positions (parenthesis) are Ba1[1a] (0, 0, 0), Ba2[2d] ($^1/_3$, $^2/_3$, *z*) with $z \approx {}^2/_3$, M^{2+}[1b] (0, 0, $^1/_2$), M^{5+}[2d] ($^1/_3$, $^2/_3$, *z*) with $z \approx {}^1/_6$, O1[3e] ($^1/_2$, 0, 0), and O2[6i] (*x*, 2*x*, *z*) with $x \approx {}^1/_6$ and $z \approx {}^1/_3$. The lattice parameters are $a \approx \sqrt{2}a_c$ and $c \approx \sqrt{3}a_c$, where a_c is the primitive cubic lattice parameter (≈4 Å) and are treated as variables in the calculation. The calculation contains six variables to optimize, namely, the two lattice parameters *a* and *c*, the three *z* coordinates of Ba2, M^{5+}, and O2, and the *x* coordinate of O2.

Each ion is initialized at the ideal fractional coordinates and the first coordination sphere interatomic distances are calculated at each grid search point. Six bond distances are calculated for M^{2+}, M^{5+} O1, and O2 and 12 for Ba1 and Ba2. Bond valences (*s*) are calculated using bond distances (*d*) with the bond valence method[29,30] according to (1)

$$s_{ij} = e^{[(R_{ij}-d_{ij})/B]} \quad (1)$$

where R_{ij} and *B* are constants. Bond valence sums (*V*) are calculated by summing the individual valence sums according to (2)

$$V_{i(calc)} = \sum_j s_{ij} \quad (2)$$

The discrepancy factors (d_i) of each ion are calculated by subtracting the bond valence sum [$V_{i(calc)}$] from the formal valence of the ion.[31] The global instability index (GII) is then calculated according to (3).[32]

$$GII = \sqrt{\frac{\sum_{i=1}^{N}(d_i^2)}{N}} \quad (3)$$

At each step of a coarse grid search, the first-coordination sphere bond distances, bond valences, bond valence sums, and GII are calculated. After the first iteration, the starting fractional coordinates and lattice parameters are retained from the optimized structure in the previous calculation loop. Multiple (3−4) iterations are performed using successively smaller search steps until the ideal calculated crystal structure is obtained. The software program executes in a Microsoft Windows platform, and typical calculation times for each composition are on the order of minutes. The structure calculation procedure selects the crystal structure with the minimum GII, simultaneously optimizing the coordination of both the cation and the anions. Optimized lattice parameters, *c*/*a* lattice parameter ratio, fractional coordinates, tolerance factors,[33] M′−O distances, and bond valence sums are shown in Table 1.

Crystal Structure Refinement. The GSAS software package[34] was used for Rietveld structural refinements using the EXPGUI interface.[35] Initial lattice parameters were obtained from the indexing of the X-ray diffraction measurements and starting fractional coordinates were obtained from SPuDS calculations shown in Table 1. Default neutron scattering lengths and cross sections were utilized in the refinements. The data were refined in the range $10° < 2\theta < 168°$ and the background was modeled using an 11-term Chebyschev polynomial. Peak profiles were modeled with a pseudo-Voight function. The M^{2+} and M^{5+} ion were initialized with partially ordered occupancies on the 1b and 2d sites. The occupancy of the B-site was then refined under the constraint $\chi[M^{5+}(1b)]\times1 + \chi[M^{5+}(2d)]\times2 = 2$ and $\chi[M^{2+}(1b)]\times1 + \chi[M^{2+}(2d)]\times2 = 1$, where χ is the fractional occupancy of the ion with the Wyckoff site shown in parentheses. The U_{iso} values were constrained to be equal for M^{2+} and M^{5+} for atoms located on the same crystallographic site. Refinement cycles involved 29−30 parameters including the scale factor, background, peak shape, unit cell, isotropic thermal parameters, and fractional coordinates. In BMN, BMT, and BNT the B-site occupancies refined to values slightly larger than unity, with an insignificant improvement in the refinement and an R_{wp} improvement of 0.02% or less. In subsequent refinements of BMN, BMT, and BNT the M^{2+} and M^{5+} cation site occupancies were fixed at unity.

(29) Brown, I. D. *Chem. Soc. Rev.* **1978**, *7*, 359.
(30) Brese, N. E.; Okeeffe, M. *Acta Crystallogr., Sect. B* **1991**, *47*, 192.
(31) Rao, G. H.; Barner, K.; Brown, I. D. *J. Phys.: Condens. Matter* **1998**, *10*, L757.
(32) Salinas-Sanchez, A.; Garcia-Munoz, J. L.; Rodriguez-Carvajal, J.; Saez-Puche, R.; Martinez, J. L. *J. Solid State Chem.* **1992**, *100*, 201.
(33) Tolerance factors were calculated using the bond-valence model to calculate ideal A−O, M−O, and M′−O bond distances, assuming 12 equidistant A−O bonds and 6 equidistant M−O and M′−O bonds. The A−O and stoichiometry weighted average M−O and M′−O bond distances are substituted in place of the sum of the ionic radii used in the tolerance factor equation.
(34) Larson, A. C.; von Dreele, R. B. *General Structure Analysis System (GSAS)*; Los Alamos National Laboratories: Los Alamos, NM, 1990.
(35) Toby, B. H. *J. Appl. Crystallogr.* **2001**, *34*, 210.

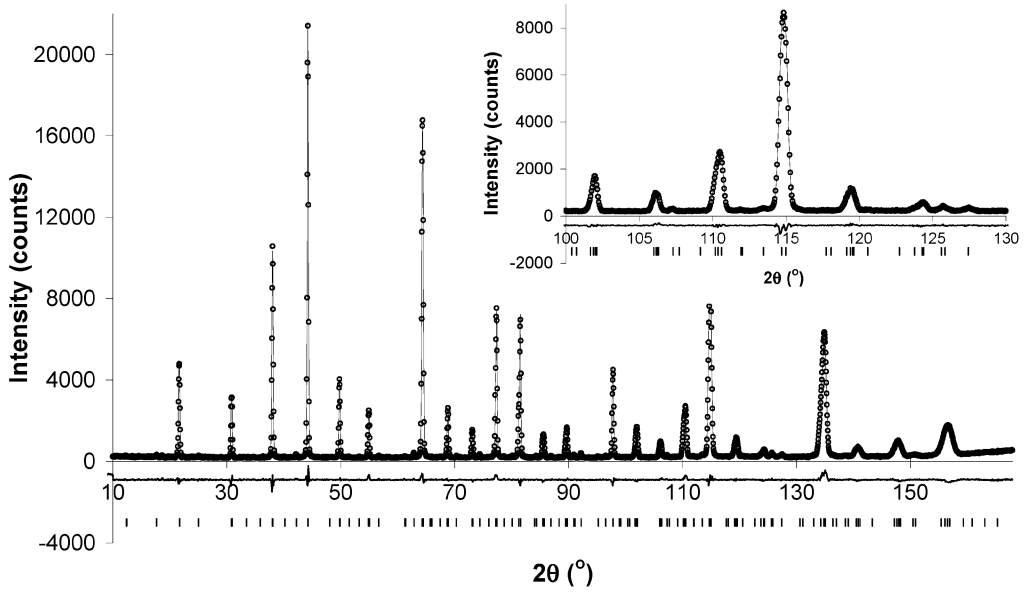

Figure 1. Observed neutron powder diffraction data (○) along with the calculated diffraction pattern (—) obtained from Rietveld refinement of $Ba_3MgTa_2O_9$. At the bottom of the figure the difference plot ($I_{obs} - I_{calc}$) is shown. Vertical bars on the bottom indicate the positions of allowed Bragg reflections. The inset shows the refined fit from 100° to 130° 2θ.

Table 2. Refined Structural Parameters, Fractional Site Occupancies, and Reliability Factors for $Ba_3MM'_2O_9$ (M = Mg, Ni, Zn; M′ = Nb, Ta)[a]

exp.	$Ba_3MgNb_2O_9$	$Ba_3MgTa_2O_9$	$Ba_3NiNb_2O_9$	$Ba_3NiTa_2O_9$	$Ba_3ZnNb_2O_9$
a (Å)	5.77544(5)	5.77385(5)	5.75496(6)	5.75513(8)	5.78207(6)
c (Å)	7.08762(9)	7.09376(8)	7.06695(9)	7.07480(11)	7.09731(11)
Ba2 z	0.6681(3)	0.6650(3)	0.6638(6)	0.6635(7)	0.6661(4)
M^{5+} z	0.1792(3)	0.1776(3)	0.1770(4)	0.1774(6)	0.1767(3)
O2 x	0.1706(1)	0.1708(1)	0.1698(2)	0.1695(2)	0.1711(1)
O2 z	0.3257(2)	0.3251(2)	0.3262(3)	0.3256(4)	0.3255(2)
f (M^{2+})/f (M^{5+}) (site 1b)	1	1	0.89(3)/0.11(3)	1	0.92(6)/0.08(6)
f (M^{5+})/f (M^{2+}) (site 2d)	1	1	0.94(2)/0.06(2)	1	0.96(3)/0.04(3)
R_p (profile) (%)	4.24	4.27	3.93	4.22	4.14
R_{wp} (weighted profile) (%)	5.25	5.30	4.87	5.35	5.27
R^2_F (Bragg) (%)	3.40	3.50	3.45	4.09	3.77
reduced χ^2 (%)	2.10	1.60	1.38	1.08	2.01

[a] The fixed atomic fractional coordinate positions are given in the text. Additional refined Rietveld fit parameters and isotropic thermal parameters are given in Supporting Information Table A.

Table 3. Selected Interatomic Distances (Å) Determined from Refined Structural Parameters of $Ba_3MM'_2O_9$ (M = Mg, Ni, Zn; M′ = Nb, Ta)[a]

	(Å)	$Ba_3MgNb_2O_9$	$Ba_3MgTa_2O_9$	$Ba_3NiNb_2O_9$	$Ba_3NiTa_2O_9$	$Ba_3ZnNb_2O_9$
×6	Ba(1)−O(1)	2.88772(3)	2.88692(3)	2.87748(3)	2.87757(4)	2.89103(3)
×6	Ba(1)−O(2)	2.8708(14)	2.8703(15)	2.8599(21)	2.8573(27)	2.8762(16)
×3	Ba(2)−O(1)	2.8830(20)	2.9024(21)	2.899(4)	2.903(4)	2.8984(22)
×3	Ba(2)−O(2)	2.9224(20)	2.9077(20)	2.889(4)	2.895(4)	2.9129(20)
×6	Ba(2)−O(2)	2.88834(6)	2.88804(9)	2.87852(14)	2.87872(17)	2.89199(8)
×3	M(5)-O(1)	2.0960(12)	2.0893(13)	2.0797(18)	2.0823(21)	2.0877(15)
×3	M(5)-O(2)	1.9307(14)	1.9331(15)	1.9416(23)	1.9405(26)	1.9382(14)
×6	M(2)-O(2)	2.1068(15)	2.1111(15)	2.0909(21)	2.0922(27)	2.1139(15)

[a] Selected interatomic angles are given in Supporting Information Table B.

Results and Discussion

Crystal Structures, Coordination, and Bonding. The refined fit of BMT to the diffraction pattern is shown in Figure 1. The Rietveld refined lattice parameters, fractional coordinates, site occupancies, and reliability factors for all compositions examined are shown in Table 2. The predicted fractional coordinates shown in Table 1 agree well with the refined values shown in Table 2, which illustrates the accuracy of the structure modeling calculations. Complete cation order was indicated for BMN, BMT, and BNT and nearly complete cation order for BNN and BZN. Selected interatomic bond distances and angles are given in Table 3. Standard uncertainties in the reported values are represented by one standard deviation. In contrast to many single and 1:1 ordered B-site cation perovskites, the crystal structures of 2:1 ordered perovskites exhibit an out-of-center distortion of M^{5+} in [$M^{5+}O_6$]. The crystal structure of $Ba_3MgTa_2O_9$ shown in Figure 2 illustrates the shift of Ta occurs toward the face of the [TaO_6] octahedra toward a neighboring layer of [MgO_6].

The source of the octahedral distortion may be understood using Pauling's Rules[36] and assuming equidistant bonds in the first coordination sphere, with each

Table 4. Number of Bonds (N), Valence of Bond (s_{M-O}), Bond Valence Sums (BVS) of Ions in $Ba_3ZnTa_2O_9$ with Distorted and Undistorted Octahedra, and the Experimental Crystal Structures

	undistorted octahedra			distorted octahedra			experimental	
	N	s_{M-O} (v.u.)	BVS (v.u.)	N	s_{M-O} (v.u.)	BVS (v.u.)	BZT21 BVS (v.u.)	BZT[22,23] BVS (v.u.)
Zn−O	6	$^1/_3$	2.0	6	$^1/_3$	2.0	2.87	1.93
Ta−O	6	$^5/_6$	5.0	3, 3	$^2/_3$, 1	5.0	3.93	4.81
O1−(Ta, Ba)	2, 4	$^5/_6$, $^1/_6$	2.33	2, 4	$^2/_3$, $^1/_6$	2.0	2.37	2.03
O2−(Zn, Ta, Ba)	1, 1, 4	$^1/_3$, $^5/_6$, $^1/_6$	1.83	1, 1, 4	$^1/_3$, 1, $^1/_6$	2.0	1.76	2.05

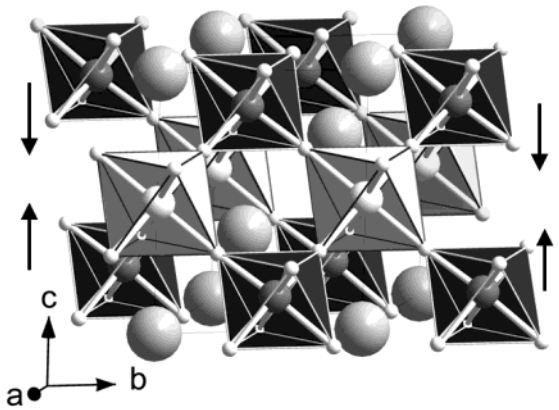

Figure 2. Crystal structure of $Ba_3MgTa_2O_9$. The large spheres represent Ba atoms and the small spheres oxygen atoms. Medium spheres represent Mg in pale [MgO_6] octahedra and Ta in dark [TaO_6] octahedra. Ta distorts out-of-center toward the octahedral face with O bonded to Mg.

cation−anion bond contributing the oxidation state divided by coordination number to the total cation bond valence sums (BVS). The cation BVS are therefore equal to the formal oxidation state using the assumption of undistorted polyhedra. However, there is an asymmetry in the bond network for the two distinctly coordinated oxygen anions with O1 bonded to 2 M^{5+} and O2 bonded to M^{2+} and M^{5+}. The $M^{5+}O_6$ has six equidistant M^{5+}−O bonds with a valence of 5/6 v.u. in the undistorted case. Three M^{5+}−O bonds may shorten and three lengthen to form bonds with valences of 2/3 and 1 v.u., respectively, which results in the BVS of the two distinct O to become equal to 2.0 v.u. and equivalent to the formal oxidation state. Bond valence sums of each crystallographically distinct O and B-site cation with undistorted and distorted TaO_6, and two experimental crystal structures of BZT are shown in Table 4. The crystal structure of BZT by Jacobson et al.[21] has BVS of O near the expected values for less distorted octahedra, whereas the Bieringer et al.[22] crystal structure has BVS of O nearer the formal oxidation state. The three short and three long M′−O bond distances from the refined structures shown in Table 3 indicate the out-of-center distortion occurs primarily in order to optimize the coordination environment of the two distinct O and are in good agreement with those predicted by the structure modeling shown in Table 1 and the BZT crystal structure by Bieringer et al.[22]

Although the out-of-center distortion primarily occurs because of the asymmetry in the bond network, the connectivity in the bond network is not the sole driving force for the distortion. In general, a distortion depends on both electronic and structural components in the nature of the bond network.[37] The highly charged d^0 Ta^{5+} or Nb^{5+} cations have low-lying d orbitals that are able to mix with the filled p orbitals of the oxygen. In the extended perovskite structure this results in a number of different electronic configurations with closely spaced energies. A spontaneous distortion can remove any near degeneracy, which is known as a second-order Jahn−Teller distortion.[38,39] In general, second-order Jahn−Teller distortions that occur for d^0 cations (e.g., Ti^{4+}, Nb^{5+}, Ta^{5+}, W^{6+}) exhibit a tendency for multiple bond lengths.[37] It is noteworthy that substitution of the similar six-coordinate ionic radius Sb^{5+} (r = 0.74 Å) for Ta^{5+} and Nb^{5+} in perovskites with a 1:1 "NaCl"-type ordered cation arrangement, which has no connectivity asymmetry for an off-center distortion, results in formation of a perovskite phase.[40] However, substitution of Sb^{5+} in 2:1 compositions with the A-site cation Ba^{2+} results in the crystallization of a phase that does not contain corner-sharing octahedra. For example, $Ba_3MSb_2O_9$ (M = Mg, Ni) crystallize in space group $P6_3/mmc$ with corner- and face-sharing octahedra.[41] The d^{10} Sb^{5+} does not have empty d orbitals to mix with the O 2p orbitals to stabilize the off-center distortion. Compositions with 2:1 ratio of B-site cations with M′ cations that contain partially filled d shells adopt a nonstoichiometric 1:1 order. Perovskites which exhibit the nonstoichiometric 1:1 order include space group $Fm\bar{3}m$, $Ba_3MM'_2O_9$ (M = Mo, W; M′ = Dy, Gd), $Ba_3WSm_2O_9$,[42] $A_3TeCo_2O_9$ (A = Sr, Ba), $Sr_3WCo_2O_9$,[43] $Sr_3WM'_2O_9$ (M′ = Cr, Fe),[44] $A_3UFe_2O_9$ (A = Sr, Ba),[45] and $Ba_3UFe_2O_9$,[46] space group $I4/m$, $Sr_3MFe_2O_9$ (M′ = Mo, W, Te, U),[47] and space group $Immm$ and $Pnnm$ $Sr_3NiSb_2O_9$.[48] Formation of 2:1 ordered perovskites appears to require a d^0 cation on the M′ site, which may undergo a second-order Jahn−Teller off-center distortion to create a more favorable coordination for the O.

(36) Pauling, L. *J. Am. Chem. Soc.* **1929**, *51*, 1010.
(37) Kunz, M.; Brown, I. D. *J. Solid State Chem.* **1995**, *115*, 395.
(38) Burdett, J. K *Molecular Shapes*; Wiley: New York, 1980.
(39) Wheeler, R. A.; Whangbo, M. H.; Hughbanks, T.; Hoffmann, R.; Burdett, J. K.; Albright, T. A. *J. Am. Chem. Soc.* **1986**, *108*, 2222.
(40) Anderson, M. T.; Greenwood, K. B.; Taylor, G. A.; Poeppelmeier, K. R. *Prog. Solid State Chem.* **1993**, *22*, 197.
(41) Treiber, U.; Kemmlersack, S. *Z. Anorg. Allg. Chem.* **1982**, *487*, 161.
(42) Fuentes, A. F.; Garza-Garcia, M.; Escalante-Garcia, J. I.; Mendoza-Suarez, G.; Boulahya, K.; Amador, U. *J. Solid State Chem.* **2003**, *175*, 299.
(43) Harari, D.; Poix, P.; Bernier, J. C *J. Solid State Chem.* **1974**, *11*, 330.
(44) Harari, D.; Poix, P. *Comput. Rend. Hebdom.* **1973**, *C276*, 265.
(45) Ropars, C.; Berthon, J. C.; Bernier, J. C.; Poix, P. *Ann. Chim. (Paris)* **1966**, 377.
(46) Berthon, J.; Grenet, J. C.; Poix, P. *Ann. Chim. (Paris)* **1979**, *8*, 609.
(47) Viola, M. D.; Augsburger, M. S.; Pinacca, R. M.; Pedregosa, J. C.; Carbonio, R. E.; Mercader, R. C. *J. Solid State Chem.* **2003**, *175*, 252.
(48) James, M.; Attfield, J. P.; Rodriguez-Carvajal, J. *J. Phys. Chem. Solids* **1995**, *56*, 1331.

Table 5. Lattice Parameter Ratio *c*/*a*, Valence (v.u.) of Long (s_l) and Short (s_s) M^{5+}−O Bonds, Average M^{5+}−O Bond Distances (Å), Octahedral Distortion Parameter (Δd), Bond Valence Sums (v.u) Calculated from Interatomic Distances in Table 4 and refs 22 and 23, GII (v.u), and Weighted Average Discrepancy Factor (⟨*d*⟩)

	$Ba_3MgNb_2O_9$	$Ba_3MgTa_2O_9$	$Ba_3NiNb_2O_9$	$Ba_3NiTa_2O_9$	$Ba_3ZnNb_2O_9$	$Ba_3ZnTa_2O_9$
c/*a*	1.2272	1.2286	1.2280	1.2293	1.2275	1.2292
s_l (v.u.)	0.606	0.633	0.634	0.645	0.620	0.644
s_s (v.u.)	0.948	0.965	0.921	0.946	0.929	0.959
Δd ($\times 10^4$)	16.9	15.1	11.8	12.4	13.8	13.4
Ba1 (v.u.)	2.41	2.41	2.48	2.49	2.38	2.33
Ba2 (v.u.)	2.31	2.30	2.36	2.34	2.28	2.27
M^{2+} (v.u.)	1.96	1.94	1.84	1.84	1.98	1.93
M^{5+} (v.u.)	4.66	4.79	4.66	4.77	4.65	4.81
O1 (v.u.)	2.00	2.04	2.05	2.07	2.01	2.03
O2 (v.u.)	2.05	2.07	2.04	2.06	2.03	2.05
GII (v.u.)	0.211	0.192	0.239	0.225	0.204	0.161
⟨*d*⟩ (v.u.)	0.048	0.079	0.058	0.084	0.037	0.059

There were additional differences observed between the M′ = Nb and M′ = Ta crystal structures. It is well-known that with increasing 2:1 cation order the *c*/*a* lattice parameter ratio becomes larger than $\sqrt{(3/2)}$.[49,50] The *c*/*a* lattice parameter ratios shown in Table 5 are slightly smaller for M′ = Nb compounds compared to the corresponding M′ = Ta in compounds, even with a similar degree of cation order. Bond valence sums were calculated using the SPuDS software with modern bond valence parameters.[51] Bond valence sums and the GII shown in Table 5 were calculated using bond distances of the refined crystal structures shown in Table 3. In each composition the tolerance factors are larger than unity, signifying the Ba^{2+} is oversized for the cavity formed by the corner-sharing [MO_6] and [$M'O_6$]. Compression of Ba^{2+} is indicated in the calculated and refined crystal structures by bond valence sums that are greater than the formal oxidation state. Conversely, the M^{2+} and M^{5+} undergo bond stretching with a decrease of the bond valence sums from ideal values. The BVS of M = Ni^{2+} for BNN and BNT show the largest deviation from two and the largest stretching of the Ni−O bonds was also predicted by the structure modeling shown in Table 1. Smaller bond valence sums are observed for M′ = Nb^{5+} compared to those for M′ = Ta^{5+}. Bond strain is distributed through both the A-site cation via compression and the B-site cations via expansion, while the O bond valence sums remain near the formal value. The GII values shown in Table 5 are large because of the significant strain in the bonds. Crystal structures are noted to have a GII as large as 0.2 v.u. in structures with lattice-induced strains, whereas crystal structures with a GII greater than 0.2 v.u. are often found to be unstable.[52] These compounds have a relatively large GII, which may also be a factor in the reason competing phases are often observed in syntheses.[53,54] The $Ba_3MM'_2O_9$ (M = Mg, Ni, Zn; M′ = Nb, Ta) compounds have a large tolerance factor and are near the edge of the perovskites stability range, which is illustrated by the formation of a nonperovskite structure type in $Ba_3MSb_2O_9$ (M = Mg, Ni) when the slightly smaller Sb^{5+} is substituted for Nb^{5+} or Ta^{5+}, but a nonstoichiometric 1:1 type ordered perovskite is observed for $Sr_3NiSb_2O_9$.

Bond valences of the short and long M^{5+}−O bonds shown in Table 5 are in good agreement with the valences of 1 v.u. and 2/3 v.u. shown in Table 4 that were predicted for distorted octahedra. The magnitude of the octahedral distortion is quantified using the octahedral distortion parameter (Δd) calculated according to (4),

$$\Delta d = \frac{1}{6}\left[\sum_{n=1,6} \frac{[d_n - (d)]}{(d)}\right]^2 \qquad (4)$$

where (*d*) is the mean M−O bond distance and d_n are the individual M−O bond distances.[55] A slightly larger distortion of the Nb^{5+} coordination environment for M = Mg, Zn is revealed by a larger Δd for M′ = Nb than for M′ = Ta shown in Table 5. Partial B-site disorder of BNN and BZN yields a slightly smaller Δd than in a fully ordered composition because of the preference of Ni^{2+} and Zn^{2+} to occupy a more symmetric octahedral coordination.

The slight differences in the coordination of Nb^{5+} and Ta^{5+} may result from differences in covalent bonding. The second-order Jahn−Teller distortion is expected to be influenced by the degree of overlap between the low-lying empty d orbitals and the filled O 2p orbitals. Electronic structure calculations and experimental measurements in a wide range of perovskite and related compounds indicate Nb^{5+} is more covalent than Ta^{5+}.[56] Calculations on $KTa_{1-x}Nb_xO_3$ also indicate more covalent bonding for Nb^{5+} and show increased preference and energy stability gain for Nb^{5+} by an off-center displacement, whereas the Ta^{5+} preferentially remained in a more symmetric environment.[57] Similar experimental coordination preferences are observed in $KTaO_3$ (space group $Pm\bar{3}m$)[58] with Ta−O bond distances (Å) of 1.994(2) ×6 and in $NaTaO_3$ (space group *Pbnm*)[59] with Ta−O bond distances (Å) 1.976(2) ×2, 1.977(2) ×2, and 1.980(2) ×2. In contrast, the bond distances (Å) in

(49) Kim, I. T.; Kim, Y. H.; Chung, S. J. *J. Mater. Res.* **1997**, *12*, 518.
(50) Kim, I. T.; Oh, T. S.; Kim, Y. H. *J. Mater. Sci. Lett.* **1993**, *12*, 182.
(51) Brown, I. D. http://www.ccp14.ac.uk/ccp/web-mirrors/i_d_brown (1/2004).
(52) Brown, I. D. *Acta Crystallogr., Sect. B* **1992**, *48*, 553.
(53) Kolodiazhnyi, T. V.; Petric, A.; Johari, G. P.; Belous, A. G. *J. Eur. Ceram. Soc.* **2002**, *22*, 2013.
(54) Kolodiazhnyi, T.; Petric, A.; Belous, A.; V'yunov, O.; Yanchevskij, O. *J. Mater. Res.* **2002**, *17*, 3182.
(55) Alonso, J. A.; Martinez-Lope, M. J.; Casais, M. T.; Fernandez-Diaz, M. T. *Inorg. Chem.* **2000**, *39*, 917.
(56) Eng, H. W.; Barnes, P. W.; Auer, B. M.; Woodward, P. M. *J. Solid State Chem.* **2003**, *175*, 94.
(57) Eglitis, R. I.; Fuks, D.; Dorfman, S.; Kotomin, E. A.; Borstel, G. *Mater. Sci. Semicond. Proc.* **2002**, *5*, 153.
(58) Zhurova, E. A.; Ivanov, Y.; Zavodnik, V.; Tsirelson, V. *Acta Crystallogr., Sect. B* **2000**, *56*, 594.
(59) Kennedy, B. J.; Prodjosantoso, A. K.; Howard, C. J. *J. Phys.: Condens. Matter* **1999**, *11*, 6319.

$KNbO_3$ (space group $Amm2$)[60] are more diverse 1.873(5) ×2, 1.996(1) ×2, and 2.169(5)×2 as the Nb^{5+} moves toward an edge. Multiple phases[61] occur for $NaNbO_3$, and the Nb−O bond distances (Å) for the room-temperature phase[62] range from 1.881(11) to 2.112(9). In a variety of structure types, the coordination environment distortion is typically larger for Nb^{5+} than for Ta^{5+}.[37] Other factors being equal, the more ionic Ta^{5+} has less driving force than the more covalent Nb^{5+} to adopt a distorted coordination environment because of the reduced mixing of the O 2p and M^{5+} d orbitals and decreased second-order Jahn−Teller distortion. The significance of the coordination differences and reduced second-order Jahn−Teller distortion on the dielectric properties is explored in the subsequent sections.

Dielectric Constant. In general, the measured ϵ are larger for Nb^{5+} than for Ta^{5+}-containing perovskites.[63,64] The increase in the ϵ results from a larger polarizability of Nb^{5+} compared to that of Ta^{5+}. Dielectric properties and average values for 2:1 perovskites in this study are shown in Supporting Information Table C and additional V_m and $\epsilon_{meas.}$ perovskite data are given in Supporting Information Table D. The average ϵ increase for $M' = Nb^{5+}$ perovskites compared to $M' = Ta^{5+}$ for Group A perovskites with a tolerance factor less than unity is 4.9(2.9), whereas the average increase for Group B perovskites with a tolerance factor larger than unity is 9.6(1.9). The larger increase of ϵ in Group B compared to Group A perovskites is attributed to a larger ionic contribution to the total polarizability resulting from the smaller BVS of Nb^{5+} than Ta^{5+}. An ion with a smaller BVS is expected to give a larger ionic polarization contribution to the ϵ because an ion with longer and weaker bonds is expected to have a more facile polarization than an ion with a more ideal BVS.

The Clausius−Mossotti (C−M) equation,[65] although strictly valid only for cubic structures in isotropic environments, may be used to estimate the ϵ of a material and is shown in (5),

$$\alpha_D = \frac{V_m(\epsilon - 1)}{b(\epsilon + 2)} \quad (5)$$

where α_D is the total dielectric polarizability, $b = 4\pi/3$, and V_m is the molar volume. The total dielectric polarizability is assumed to be equal to the sum of individual ion polarizabilities determined from dielectric data of single-crystal oxides and fluorides and noncubic compounds if the dielectric anisotropy was determined.[18] The agreement between the C−M equation calculated ϵ with the measured ϵ was approximately 0.5% in well-behaved compounds. In nonisotropic perovskite structures the macroscopic polarizability not only is the sum of the ion polarizabilities but also contains additional components from the crystal structure. C−M calculated ($\epsilon_{calc.}$) and measured ($\epsilon_{meas.}$) dielectric constants are plotted in Figure 3. There is relatively good agreement

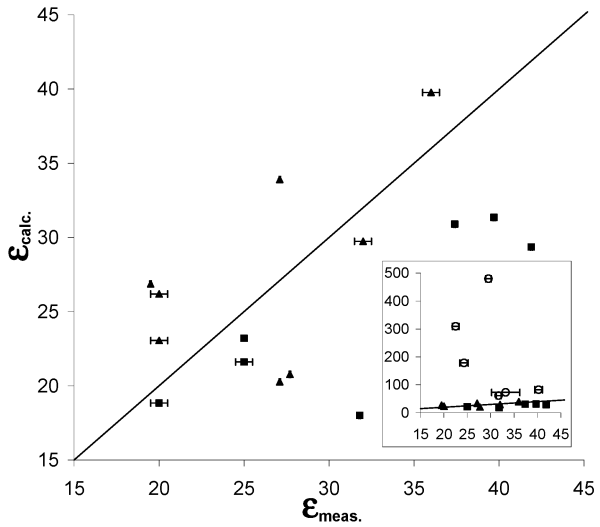

Figure 3. C−M equation calculated ($\epsilon_{calc.}$) versus experimental ($\epsilon_{meas.}$) dielectric constants. The line represents $\epsilon_{calc.} = \epsilon_{meas.}$. Squares represent $M' = Nb$, triangles represent $M' = Ta$ for Group A (tol. < 1) perovskites, and circles represent Group B (tol. > 1) perovskites. The inset has the same axis labels. Error bars represent one standard deviation. The full list of compounds in this figure may be found in the Supporting Information Table D.

Table 6. Average τ_f, Maximum $Q\times f$, Experimental $\epsilon_{meas.}$ and Calculated $\epsilon_{calc.}$ and ϵ_s Using Experimental and SPuDS Molar Volumes, Respectively[a]

	τ_f (10^{-6} K^{-1})	$(Q\times f)_{max}$ (THz)	$\epsilon_{meas.}$	$\epsilon_{calc.}$	ϵ_s
$Ba_3MgNb_2O_9$	25(8)	160(5)	31.7(4)	61	39
$Ba_3MgTa_2O_9$	3(2)	430(5)	24.3(9)	180	66
$Ba_3NiNb_2O_9$	−12(7)	48.0(5)	33(3)	73	41
$Ba_3NiTa_2O_9$	−14(3)	95.50(5)	22.5(5)	312	71
$Ba_3ZnNb_2O_9$	27(4)	86.90(5)	40.3(8)	83	49
$Ba_3ZnTa_2O_9$	0.9(2)	168(5)	29.5(5)	483	94

[a] One standard deviation is given in parentheses using data contained in Supporting Information Table A.

in the calculated and measured dielectric constants for Group A (tol. < 1) perovskites, but significant error with Group B (tol. > 1) perovskites shown in the inset. One source of the discrepancy is the relatively small V_m of the Group B perovskites; the V_m are much smaller than expected from the predicted lattice parameters, which is illustrated by comparing Tables 1 and 2. The ϵ_s calculated using the V_m from SPuDS modeling and standard ion polarizabilities are in better agreement with ϵ_{meas} shown in Table 6. The constraints imposed by the corner-sharing octahedra and the resulting compression of the A-site and slight expansion of the B-site results in an overall compression in the bonds, with the sum of the discrepancy factors being larger than zero. The weighted average discrepancy factor ($\langle d \rangle$) gives the average deviation from ideal bond valence sums and was calculated by using the following eq 6,

$$\langle d \rangle = \frac{\sum_i^n w_i d_i}{N} \quad (6)$$

where w is the Wyckoff site multiplicity, d_i is the discrepancy factor for each of the n ions on a distinct crystallographic site, and N is the number of atoms in

(60) Hewat, A. W. *J. Phys. C: Solid State Phys.* **1973**, *6*, 2559.
(61) Darlington, C. N. W.; Knight, K. S. *Physica B* **1999**, *266*, 368.
(62) Sakowski-Cowley, A. C.; Lukaszewicz, K.; Megaw, H. D. *Acta Crystallogr., Sect. B* **1969**, *B25*, 851.
(63) Kagata, H.; Kato, J. *Jpn. J. Appl. Phys. 1* **1994**, *33*, 5463.
(64) Takata, M.; Kageyama, K. *J. Am. Ceram. Soc.* **1989**, *72*, 1955.
(65) Bosman, A. J.; Havinga, E. E. *Phys. Rev. B: Condens. Matter* **1963**, 192.

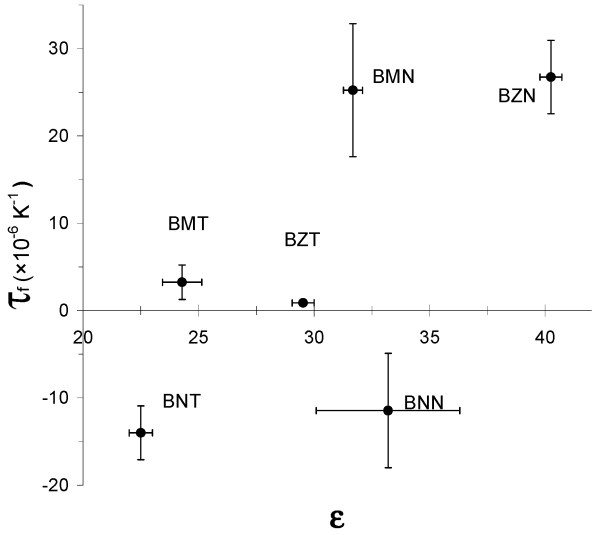

Figure 4. Average τ_f versus average ϵ. Error bars represent one standard deviation.

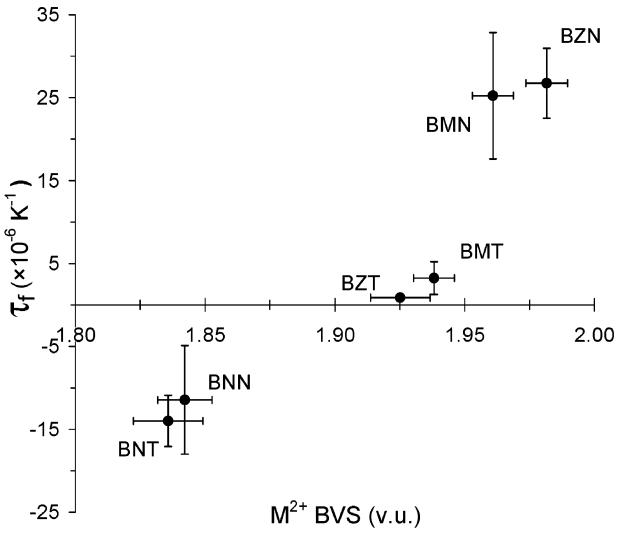

Figure 5. Average τ_f versus M^{2+} bond valence sum. Error bars represent one standard deviation.

the unit cell. The positive $\langle d \rangle$ values listed in Table 5 indicate the ions are, on average, over-bonded.

The similar M^{5+} ionic radii and V_m, but larger ϵ of Nb^{5+} compared to Ta^{5+} perovskites leads one to expect a larger ion polarizability for Nb^{5+}. However, the tabulated ion polarizabilities[18] are $\alpha(Nb^{5+}) = 3.97$ Å^3 and $\alpha(Ta^{5+}) = 4.73$ Å^3. These values are inaccurate relative to each other for use in perovskites. The calculation of Nb^{5+} and Ta^{5+} ion polarizabilities applicable for perovskites was obtained using only compositions from Group A to calculate the total dielectric polarizabilities. With use of the C−M equation and the experimental V_m and ϵ, the ion polarizabilities of Nb^{5+} and Ta^{5+} for each composition were calculated by subtracting standard ion polarizabilities of the non-M^{5+} ions from the C−M calculated total dielectric polarizability. Updated average ion polarizabilities values for Nb^{5+} and Ta^{5+} are 4.65(80) and 4.55(89) Å^3, respectively. The average ion polarizability value obtained for Nb^{5+} exhibits the largest deviation from the tabulated value, whereas the value for Ta^{5+} is in closer agreement. The updated ion polarizabilities for Nb^{5+} and Ta^{5+} may only be usable for well-behaved perovskite systems with a tolerance factor less than unity and may not be applicable to other structure types.

Temperature Coefficient of the Resonant Frequency (τ_f). The τ_f is related to the temperature coefficient of the dielectric constant (τ_ϵ) and the linear thermal expansion coefficient (α_l) by $\tau_f = -1/2(\tau_\epsilon + \alpha_l)$. Low ϵ materials typically have a positive τ_ϵ, and high ϵ materials (>20) generally have a more negative τ_ϵ.[66,17] Assuming a typical α_l for perovskites, a larger ϵ and more negative τ_ϵ is expected to result in a more positive τ_f and has been observed previously in a wide range of dielectrics.[67,68,69] For the 2:1 perovskites examined in this study, the general trend of more positive τ_f with increasing ϵ is also observed and shown in Figure 4. However, the general relationship between τ_f and ϵ does not rationalize the relatively large τ_f differences observed between BNT and BMT and BNN, BMN, and BZT, which respectively have similar ϵ. In these compounds, ion coordination and bonding are proposed to be the source of the difference in τ_f.[69] The most significant coordination difference is in M^{2+} and the BVS of M^{2+} versus τ_f shown in Figure 5. The coordination of M^{2+} displays a trend in which a more underbonded (smaller BVS) M^{2+} exhibits a more negative τ_f.

The M^{2+}−O and M^{5+}−O bond lengths change at different rates. In general, for the same coordination number, the M−O bond distances change more slowly with temperature for higher valent (i.e., M^{5+}) ions than for lower valent (i.e., M^{2+}) ions.[70] This will change the polarizability differently at each B-site and hence ϵ and τ_f with temperature. The A-site is over-bonded and the O has nearly ideal bonding; therefore, the ionic component of the polarization is not expected to change as significantly with temperature as the underbonded B-site cations. A detailed analysis of the differences in the chemistry and bonding influences on the τ_f of the alkaline earth (Mg^{2+}), d^8 transition metal (Ni^{2+}), or the full d^{10} shell (Zn^{2+}) cations would need to be considered in a comprehensive analysis of the structure−property relationships. However, the coordination trends are a useful guide in understanding the dielectric property differences and may be used to estimate the τ_f for space group $P\bar{3}m1$ perovskites based on the ϵ and atomic coordination environment of M^{2+}.

Dielectric Loss and $Q\times f$. Extracting the primary influences on Q values is difficult because of the complexity of separating intrinsic (e.g., cation order and phonon modes) and extrinsic (e.g., defects, impurity, processing, and sintering conditions) contributions to dielectric loss. Intrinsic dielectric loss originates from anharmonic interactions of the electric field with the phonon system.[71] The $Q\times f$ product is approximately equal for measurements performed on samples with different sizes and enables a comparison of Q measured

(66) Cockbain, A. G.; Harrop, P. J. *Br. J. Appl. Phys. D* **1968**, *1*, 1109.
(67) Wersing, W. *Curr. Opin. Solid State Mater. Sci.* **1996**, *1*, 715.
(68) Wise, P. L.; Reaney, I. M.; Lee, W. E.; Price, T. J.; Iddles, D. M.; Cannell, D. S. *J. Eur. Ceram. Soc.* **2001**, *21*, 2629.
(69) Wise, P. L.; Reaney, I. M.; Lee, W. E.; Iddles, D. M.; Cannell, D. S.; Price, T. J. *J. Mater. Res.* **2002**, *17*, 2033.
(70) Brown, I. D.; Dabkowski, A.; McCleary, A. *Acta Crystallogr., Sect. B* **1997**, *53*, 750.
(71) Gurevich, V. L.; Tagantsev, A. K. *Adv. Phys.* **1991**, *40*, 719.

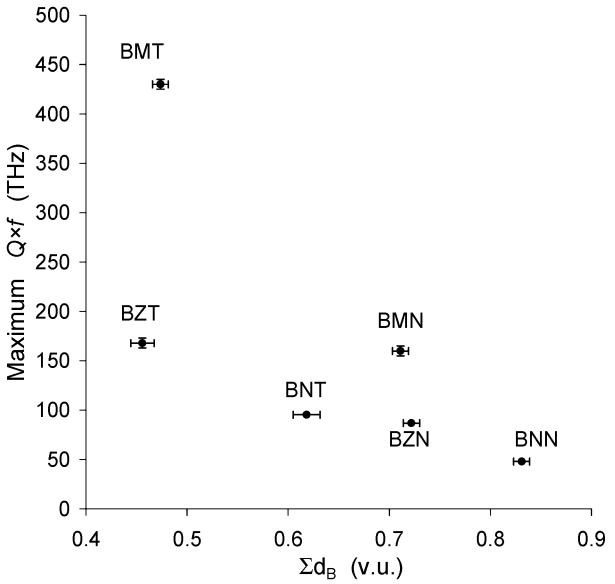

Figure 6. Maximum reported $Q \times f$ versus sum of B-site cation discrepancy factors (Σd_i). Error bars represent one standard deviation.

at different frequencies. The large variance in $Q \times f$ observed in ceramics shown in the large standard deviation in Supporting Information Table C results from the combination of both intrinsic and extrinsic effects. In many systems it is possible that slightly higher $Q \times f$ could be obtained with additional processing studies; however, considering the significant research on the 2:1 perovskites, the maximum reported $Q \times f$ values are very likely to be near the optimal intrinsic values.

An interesting correlation is observed with the sum of the differences between the B-site cation calculated BVS and the formal oxidation state $\Sigma d_B = \{2 \times [5 - \mathrm{BVS}(M^{5+})] + [2 - \mathrm{BVS}(M^{2+})]\}$. The smaller the sum of the B-site discrepancy factors, the higher the maximum reported $Q \times f$ values shown in Figure 6. Weakly bonded B-site cations in an expanded coordination environment may be one source of intrinsic dielectric loss. In a classical sense the more under-bonded B-site ions contribute to the dielectric loss because the ions "rattle" more freely in the octahedral cage and may interact more strongly with the anharmonic phonons. The precise nature of the contribution of the expanded coordination environment of $[MO_6]$ and $[M'O_6]$ to the dielectric loss is beyond the scope of this paper, but the correlation is presented to base future efforts on understanding intrinsic sources of dielectric loss in the 2:1 ordered perovskites.

Conclusions

Crystal structures of five $Ba_3MM'_2O_9$ (M = Mg, Ni, Zn; M′ = Nb, Ta) isostructural perovskites with 2:1 B-site ordering are reported from Rietveld refinements of neutron powder diffraction data. The perovskites crystallize in space group $P\bar{3}m1$ with ordered (111) planes of M and M′ cations with a {M′M′M} layer repeat unit. Crystal structure modeling was used to generate a starting structural model for the Rietveld refinements. Constraints imposed by the space group symmetry combined with the optimization of the GII allow accurate prediction of the fractional coordinates. The coordination environments of Ba^{2+} are compressed and the $[MO_6]$ and $[M'O_6]$ octahedra are expanded, resulting in bond valence sums that are larger for Ba^{2+} and smaller for M^{2+} and M^{5+} than the formal oxidation states, whereas the O BVS are near ideal values. The modeling predicts the d^0 cations (i.e., Ta^{5+} and Nb^{5+}) shift out of the center of the $[M'O_6]$ octahedron, forming three short and three long M′−O bonds, which is analogous to the experimental distortion.

Both of the M′ = Nb^{5+} and Ta^{5+} B-site cations undergo an out-of-center distortion to simultaneously satisfy the coordination requirements of both the O and cations. The out-of-center distortion is driven by the bond connectivity asymmetry and is allowed electronically by the second-order Jahn−Teller distortion of the d^0 M′ cations. The 2:1 ordered perovskite is not observed by substituting a d^{10} M′ = Sb^{5+} or 2:1 compositions with partially occupied d orbitals on the M′ cation; instead, other structures types or non-2:1 ordering is observed. Electronic contributions to bonding should be considered in experimental efforts to manipulate dielectric properties via B-site substitution to retain the high-Q 2:1 ordered state, rather than the lower-Q 1:1 ordered state of perovskites. The more covalent Nb^{5+} has a higher preference for occupying a more distorted coordination environment revealed by an enhanced off-center shift (i.e., increased Δd), while Ta^{5+} typically crystallizes with a more symmetric coordination environment. The observed coordination environment combined with smaller bond valence sums of Nb^{5+} is used to suggest a more facile ionic polarization is present for the M′ = Nb^{5+} perovskites. A larger ionic polarization component to the total polarizability of M′ = Nb^{5+} is present compared to that of M′ = Ta^{5+}, resulting in a larger measured ϵ. A detailed bond valence analysis reveals similar Ba and O coordination between compositions, and interesting relationships of the B-site coordination environments and dielectric properties. In addition to the general increase in τ_f with an increase in ϵ, a composition with a smaller bond valence sum of M^{2+} exhibits a more negative τ_f. The smaller the sum of the discrepancy factors for the B-site correlates well with a larger measured $Q \times f$ maximum. The phenomenological relationships presented here are also a potential starting point in further investigations into the crystal structure−dielectric property relationships of 2:1 ordered perovskites.

Acknowledgment. This work was supported in part by a postdoctoral fellowship administered by the National Research Council. The author thanks T. A. Vanderah and P. W. Barnes for useful discussions.

Supporting Information Available: Crystallographic information files (CIF) for $Ba_3MgNb_2O_9$, $Ba_3MgTa_2O_9$, $Ba_3NiNb_2O_9$, $Ba_3NiTa_2O_9$, and $Ba_3ZnNb_2O_9$. Table containing Rietveld refinement parameters and isotropic thermal parameters; table containing selected bond angles; table containing ϵ, τ_f, and $Q \times f$ for 2:1 perovskites; table containing $\epsilon_{meas.}$, V_m, ϵ_{calc}, α, and references for Group A and Group B perovskites (PDF). This material is available free of charge via the Internet at http://pubs.acs.org.

CM049831K